
Mathematical Modelling and Analysis
Volume 24, Issue 2, 179–194, 2019
https://doi.org/10.3846/mma.2019.013

http://mma.vgtu.lt
ISSN: 1392-6292
eISSN: 1648-3510

# Verification of an Entropy Dissipative QGD-Scheme for the 1D Gas Dynamics Equations

**Alexander Zlotnik**[a] **and Timofey Lomonosov**[a]

[a] *National Research University Higher School of Economics*
101000 Moscow, Myasnitskaya str., 20
E-mail(*corresp.*): azlotnik@hse.ru
E-mail: tlomonosov@hse.ru

Received September 25, 2018; revised January 6, 2019; accepted January 6, 2019

**Abstract.** An entropy dissipative spatial discretization has recently been constructed for the multidimensional gas dynamics equations based on their preliminary parabolic quasi–gasdynamic (QGD) regularization. In this paper, an explicit finite-difference scheme with such a discretization is verified on several versions of the 1D Riemann problem, both well-known in the literature and new. The scheme is compared with the previously constructed QGD-schemes and its merits are noticed. Practical convergence rates in the mesh $L^1$-norm are computed. We also analyze the practical relevance in the nonlinear statement as the Mach number grows of recently derived necessary conditions for $L^2$-dissipativity of the Cauchy problem for a linearized QGD-scheme.

**Keywords:** 1D gas dynamics equations, entropy dissipative spatial discretization, explicit finite-difference scheme, verification on the Riemann problem, practical stability analysis.

**AMS Subject Classification:** 65M06; 65M12; 76N99.

## 1 Introduction

Vast literature is devoted to methods for numerical solving gas dynamics equations, see, in particular, [1, 10, 11, 16]. In recent years, those methods that are in addition entropy dissipative (conservative) attract much attention, see, in particular, [1, Ch. 18, 19], [6, 8, 13, 14, 15, 17].

The quasi-gasdynamic (QGD) system of equations [2, 3] is an entropy-correct and the Petrovsky parabolic [18, 21] regularization of the gas dynamics equations. It serves as the basis for constructing a family of QGD-finite-

difference schemes to solve the latter equations. Such schemes have been successfully used since the mid-1980s in a wide variety of applied computations.

Entropy dissipative spatial QGD-discretizations were first constructed and verified in the 1D case in [7,19]. Also such a QGD-discretization has recently been constructed in the multidimensional case [20]. In the present paper, the explicit finite-difference scheme with this discretization is verified in the 1D case on several versions of the Riemann problem on the disintegration of a discontinuity, both well-known in the literature [12,15] and new. The scheme is compared with previously constructed standard-type QGD-schemes, and its merits are noticed that include, in some tests, obtaining numerical solutions of better quality (on the same grid) and/or possibility to use larger time steps (occasionally tens and hundreds times more). In addition, practical convergence rates in the mesh $L^1$-norm are computed for a typical discontinuous solution, and it is shown that they are close to 0.5. We note that, for the entropy dissipative QGD-discretizations, in addition, the kinetic and internal energy balance equations contain no any indefinite non-divergent mesh imbalances [7,19,20] whereas all known standard-type QGD-schemes possess no these properties.

Both necessary and sufficient conditions for $L^2$-dissipativity of the Cauchy problem for a linearized QGD-scheme have recently been derived in [22]. In the last part of the paper, we also analyze the practical relevance of the necessary conditions in the nonlinear statement as the Mach number grows on a version of the Riemann problem and show that it is valid, within certain limits, with better quality for the entropy dissipative QGD-discretization.

## 2 The quasi-gasdynamic system of equations and related schemes for the 1D gas dynamics equations

The quasi-gasdynamic (QGD) system of equations [2,3] in the 1D case consists of the following mass, momentum and total energy balance equations

$$\partial_t \rho + \partial_x j = 0, \tag{2.1}$$

$$\partial_t (\rho u) + \partial_x (ju + p) = \partial_x \Pi, \tag{2.2}$$

$$\partial_t E + \partial_x \left[(E + p)(u - w)\right] = \partial_x (-q + \Pi u), \tag{2.3}$$

where $\partial_t$ and $\partial_x$ are the partial derivatives in time $t \geq 0$ and spatial coordinate $x \in \mathbb{R}$. The functions $\rho > 0$, $u$, $E = 0.5\rho u^2 + \rho\varepsilon$ are respectively the gas density, velocity and total energy as well as $p$ and $\varepsilon > 0$ are the pressure and specific internal energy. We take the perfect polytropic gas state equation $p = (\gamma - 1)\rho\varepsilon$, $\gamma = \text{const} > 1$, and exclude the absolute temperature from consideration.

In these equations, the mass flux $j$ together with the regularizing velocities $w$ and $\widehat{w}$, viscous stress $\Pi$ and heat flux $q$ are as follows

$$j = \rho(u - w), \quad w = \frac{\tau}{\rho}\partial_x(\rho u^2 + p), \quad \widehat{w} = \frac{\tau}{\rho}(\rho u \partial_x u + \partial_x p), \tag{2.4}$$

$$\Pi = \mu \partial_x u + \rho u \widehat{w} + \tau(u \partial_x p + \gamma p \partial_x u), \tag{2.5}$$

$$-q = \widetilde{\varkappa}\partial_x \varepsilon + \tau\rho\Big(\partial_x \varepsilon + p\partial_x \frac{1}{\rho}\Big)u^2. \tag{2.6}$$

Here $\tau = \tau(\rho, u, \varepsilon) > 0$ is the regularizing parameter, and the coefficients of artificial viscosity $\mu$ and (scaled) heat conductivity $\widetilde{\varkappa}$ are given by the formulas

$$\mu = \alpha_S \tau p, \quad \widetilde{\varkappa} = \gamma \mu / \alpha_P, \tag{2.7}$$

where $\alpha_S > 0$ and $\alpha_P > 0$ are respectively the Schmidt and Prandtl numbers.

We define the uniform mesh $\omega_h$ on $\mathbb{R}$ with the nodes $x_k = kh$, $k \in \mathbb{Z}$, and the step $h = X/N$, where $X > 0$. Let $\omega_h^*$ be the auxiliary mesh with the nodes $x_{k-1/2} = (k - 1/2)h$, $k \in \mathbb{Z}$. Let $\bar{\omega}^{\Delta t}$ be the mesh in $t$ with the nodes $0 = t_0 < t_1 < \ldots < t_m < \ldots$ and the steps $\Delta t_m = t_{m+1} - t_m$, $m \geq 0$. We set $v_k^m = v(x_k, t_m)$, $y_{k-1/2}^m = y(x_{k-1/2}, t_m)$.

We define the mean value, shift and finite-difference mesh operators in $x$ and $t$

$$sv_{k-1/2} = \frac{v_{k-1} + v_k}{2}, \; v_{-,k-1/2} = v_{k-1}, \; v_{+,k-1/2} = v_k, \; \delta v_{k-1/2} = \frac{v_k - v_{k-1}}{h},$$
$$\delta^* y_k = \frac{y_{k+1/2} - y_{k-1/2}}{h}, \quad \delta_t v^m = \frac{v^{m+1} - v^m}{\Delta t_m}.$$

We consider three two-level explicit in time and three-point symmetric in space QGD-schemes. The scheme $\mathcal{S}$ with the standard-type spatial discretization [19] has the form

$$\begin{aligned}
&\delta_t \rho + \delta^* j = 0,\\
&\delta_t(\rho u) + \delta^*(jsu + sp) = \delta^* \Pi,\\
&\delta_t E + \delta^*\big[\big(E^{(0)} + sp\big)\big(su - w\big)\big] = \delta^*(-q + \Pi su).
\end{aligned}$$

Hereafter the main equations (2.1)–(2.3) are approximated in space on the mesh $\omega_h$, and the main sought functions $\rho$, $u$ and $\varepsilon$ as well as the functions $E$ and $p$ are also defined on $\omega_h$.

Functions (2.4)–(2.6) are approximated in space on the mesh $\omega_h^*$:

$$\begin{aligned}
j &= s\rho \cdot (su - w), \quad w = \frac{\tau_*}{s\rho}\,\delta(\rho u^2 + p), \quad \widehat{w} = \frac{\tau_*}{s\rho}\big(s\rho \cdot su \cdot \delta u + \delta p\big),\\
\Pi &= s\mu \cdot \delta u + s\rho \cdot su \cdot \widehat{w} + \tau_*\big(su \cdot \delta p + \gamma sp \cdot \delta u\big),\\
-q &= s\widetilde{\varkappa} \cdot \delta\varepsilon + \tau_* s\rho \cdot \Big(\delta\varepsilon + sp \cdot \delta\frac{1}{\rho}\Big)(su)^2.
\end{aligned}$$

Hereafter, to reduce the amount of brackets, we assume that, for example, $s\rho \cdot (su - w) = (s\rho)(su - w)$ (i.e., the sign $\cdot$ terminates the action of the preceding operators on the left).

Also $E^{(0)} = \frac{1}{2}(s\rho)(su)^2 + s(\rho\varepsilon)$ and $\tau_* = s\tau$ on $\omega_h^*$, where the regularizing parameter $\tau$ is defined on $\omega_h$ by one of the formulas

$$(a)\ \tau = \alpha h / c_s \ \text{ or } \ (b)\ \tau = \widehat{\alpha} h / (|u| + c_s), \tag{2.8}$$

where $\alpha > 0$ and $\widehat{\alpha} > 0$ are parameters (normally $\alpha \leq 0.5$ and $\widehat{\alpha} < 1$), $c_s = \sqrt{\gamma(\gamma - 1)\varepsilon}$ is the sound velocity. Formulas (2.7) are in use on $\omega_h$.

The time step is chosen as

$$\Delta t = \beta h / \max_{\omega_h}(|u| + c_s)$$

in all the schemes, where $0 < \beta \le 1$ is a parameter (the Courant number).

The scheme $\mathcal{S}$ (and other standard-type QGD-schemes, see below) possesses no the property of entropy dissipativity since its entropy balance equation contains indefinite non-divergent mesh imbalances [19].

The scheme $\mathcal{A}$ with the entropy dissipative spatial discretization from [19] has the form

$$\delta_t \rho + \delta^* j = 0, \tag{2.9}$$

$$\delta_t(\rho u) + \delta^*(jsu + sp) = \delta^* \Pi, \tag{2.10}$$

$$\delta_t E + \delta^*\big[(E^{(1)} + sp)(su - w) - 0.25h^2 \delta u \cdot \delta p\big] = \delta^*(-q + \Pi su). \tag{2.11}$$

Functions (2.4)–(2.6) are approximated as follows

$$j{=}\rho_{\ln}(su - w),\ \ w{=}\widehat{w} + \frac{\tau_*}{s\rho}\, su \cdot \delta(\rho u),\ \ \widehat{w} = \frac{\tau_*}{s\rho}\,(s\rho \cdot su \cdot \delta u + \delta p), \tag{2.12}$$

$$\Pi = s\mu \cdot \delta u + s\rho \cdot su \cdot \widehat{w} + \tau_*\big(su \cdot \delta p + \gamma(sp)_1 \delta u\big), \tag{2.13}$$

$$-q = s\widetilde{\varkappa} \cdot \delta\varepsilon + \tau_* s\rho \cdot \Big(\delta\varepsilon - \frac{(sp)_1}{(s\rho)^2}\delta\rho\Big)(su)^2. \tag{2.14}$$

In addition, the following non-standard formulas are applied

$$E^{(1)} = 0.5\rho_{\ln} u_- u_+ + \rho_{\ln}\varepsilon^{\ln},\ \ (sp)_1 = (\gamma - 1)s\rho \cdot s\varepsilon, \tag{2.15}$$

$$\rho_{\ln} = 1/\ln(\rho_-; \rho_+),\ \ \varepsilon^{\ln} = \varepsilon_-\varepsilon_+ \ln(\varepsilon_-; \varepsilon_+). \tag{2.16}$$

Here the non-standard means $\rho_{\ln}$ and $\varepsilon^{\ln}$ play an essential role, with the difference quotient for the logarithmic function

$$\ln(a; b) = \frac{\ln b - \ln a}{b - a} \ \text{ for } \ a \ne b,\ \ \ln(a; a) = \frac{1}{a},\ \ a > 0,\ \ b > 0.$$

To avoid loss of accuracy for $|b/a - 1| \le \delta$, with $\delta > 0$ small enough, the Simpson rule for the corresponding integral is used:

$$\ln(a; b) = \int_0^1 \frac{d\alpha}{(1 - \alpha)a + \alpha b} \approx \frac{1}{6a} + \frac{4}{3(a + b)} + \frac{1}{6b}.$$

In [7], this discretization was generalized to the case of general state equations, and it was verified for the perfect polytropic gas and more complex state equations on a set of known tests. Unfortunately, there exists no its direct generalization to the multidimensional case.

Also two simplified schemes $\mathcal{A}$ are considered below: the scheme $\mathcal{A}_1$ with the means $\rho_{\ln}$ and $\varepsilon^{\ln}$ replaced by the simplest ones $s\rho$ and $s\varepsilon$ as well as the scheme $\mathcal{A}_2$, where in addition $u_- u_+$ is replaced by $(su)^2$ (in $E^{(1)}$) and the term $-0.25h^2 \delta u \cdot \delta p$ is omitted in equation (2.11).

The entropy dissipative spatial discretization has recently been constructed for the multidimensional QGD-equations in [20]. In the 1D case, it leads to the scheme $\mathcal{B}$ where the same equations (2.9)–(2.11) and the formulas $j = \rho_{\ln}(su - w)$ and (2.15)–(2.16) are used. But the other functions (2.4)–(2.6) are discretized alternatively:

$$w = \widehat{w} + A_\varepsilon \frac{s(\tau\rho)}{(s\rho)^2}\, su \cdot \delta(\rho u), \quad \widehat{w} = A_\varepsilon \frac{s\varepsilon}{(s\rho)^2}\, s\left(\frac{\tau\rho}{\varepsilon}\right)\big(s\rho \cdot su \cdot \delta u + \delta p\big),$$

$$\mathit{\Pi} = s\mu \cdot A_\varepsilon \delta u + su \cdot s\rho \cdot \widehat{w} + A_\varepsilon \frac{s(\tau\rho)}{s\rho}\big(su \cdot \delta p + \gamma(sp)_1 \delta u\big),$$

$$-q = s\widetilde{\varkappa} \cdot \delta\varepsilon + A_\varepsilon s(\tau\rho) \cdot \Big(\delta\varepsilon - \frac{(sp)_1}{(s\rho)^2}\delta\rho\Big)(su)^2,$$

where $A_\varepsilon = \varepsilon_-\varepsilon_+/(s\varepsilon)^2$. Notice that the latter formulas are essentially transformed in comparison with the original version [20] in order to make them closer to (2.12)–(2.14).

All the described schemes are originally constructed and analyzed on a non-uniform mesh $\omega_h$.

## 3 Computations of the Riemann problem and comparison of schemes

Traditionally, the Riemann problem is widely used to analyze the properties of numerical methods for solving the gas dynamics equations. The initial data are piecewise-constant and discontinuous in it. Below we consider five tests which are versions of this problem and reflect different situations in the arising flows. The tests 1–4 are well-known in the literature [4, 5, 9, 12, 16], and test 5 has recently been proposed to us by M.V. Kraposhin.

**Table 1.** Data for the Riemann problem

| No. | $\rho_L$ | $u_L$ | $p_L$ | $\rho_R$ | $u_R$ | $p_R$ | $t_{fin}$ |
|---|---|---|---|---|---|---|---|
| 1 | 1 | 0.75 | 1 | 0.125 | 0 | 0.1 | 0.2 |
| 2 | 1 | -2 | 0.4 | 1 | 2 | 0.4 | 0.15 |
| 3 | 5.99924 | 19.5975 | 460.894 | 5.99924 | -6.19633 | 46.095 | 0.035 |
| 4 | 0.1261192 | 8.9047029 | 782.92899 | 6.591493 | 2.2654207 | 3.1544874 | 0.0039 |
| 5a | 0.5 | 10 | 0.5 | 1 | -10 | 1 | 0.03 |
| 5b | 0.05 | 10 | 0.05 | 1 | -10 | 1 | 0.03 |

In Table 1, the values of initial data (for $t = 0$) in the tests left and right of the discontinuity for $x = 0$ are labeled with the indices $L$ and $R$ respectively, and $t_{fin}$ is the computation time. It is taken $\gamma = 1.4$ in tests 1–4 and $\gamma = 5/3$

in test 5. We use formula (2.8)(a) in tests 1–4 (for continuity with [4,5]) and (2.8)(b) in test 5.

The tests are treated on the segment $[-X/2, X/2]$ with $X = 1$ and for $\alpha_S = \alpha_P = 1$; for even $N$, at $x = 0$ the initial values of $v = \rho, u, \varepsilon$ are taken as $(v_L + v_R)/2$. Define the mesh $\omega_{Xh} = \{-X/2 + kh\}_{k=0}^{N}$ with $h = X/N$.

Below we present some brief information on solving these tests by the schemes $\mathcal{S}$, $\mathcal{A}$, $\mathcal{A}_1$, $\mathcal{A}_2$ and $\mathcal{B}$ as well as also by the standard-type QGD-scheme $S_0$ from [4,5], which is somewhat different from the scheme $\mathcal{S}$. Note that the verification of one more standard-type QGD-scheme and its comparison with the Kurganov-Tadmor scheme has recently been performed in [9].

*Test 1.* This test is one of the Sod problem versions. In the arising flow with discontinuities, there are typical elements such as a rarefaction wave, a contact discontinuity and a shock wave. The results of computations are shown in Figure 1. It and similar figures below contain graphs of the approximate functions $v$ for the scheme $\mathcal{B}$ of our main interest (solid line) and, for comparison, the exact functions $v_{ex}$ (dashed line), where $v = \rho, u, p, \varepsilon$, at time $t_{fin}$.

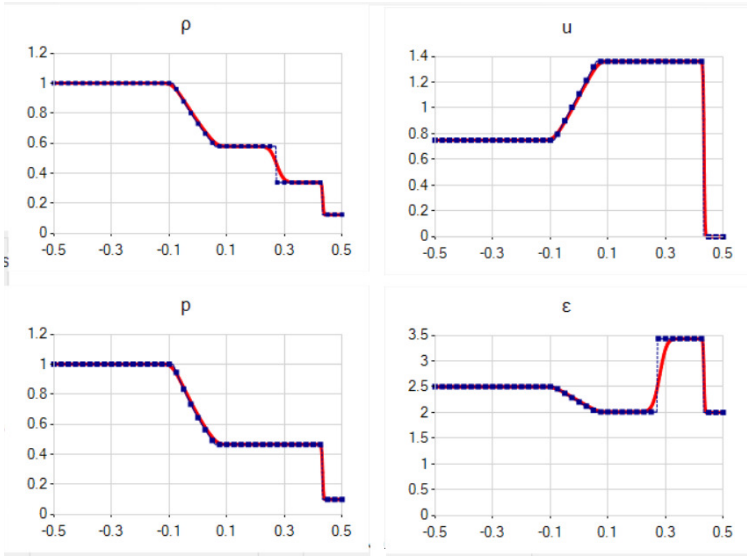


**Figure 1.** Test 1. Solutions for $\alpha = 0.2$, $\beta = 0.3$ and $N = 400$

For all schemes $\mathcal{S}$, $\mathcal{A}$, $\mathcal{A}_1$, $\mathcal{A}_2$ and $\mathcal{B}$, the results are close. In particular, for $\alpha = 0.3$ and $N = 400$, the value $\beta = 0.7$ is admissible for them whereas the smaller value $\beta = 0.4$ was taken for the scheme $S_0$ in [5].

In this test, we also analyze practical orders of convergence. We introduce the $L^1$-norm of a function $v$ defined on the mesh $\omega_{Xh}$:

$$\|v\|_{L_h^1} = \frac{h}{2}|v_0| + h\sum_{k=1}^{N-1}|v_k| + \frac{h}{2}|v_N|.$$

The relative $L_h^1$-error of the approximate function $v$ is calculated by the formula

$$r_h(v) = \|v - v_{ex}\|_{L_h^1} / \|v_{ex}\|_{L_h^1},$$

where $v_{ex}$ is the exact value of the function $v = \rho, u, \varepsilon$.

We select the set of values $N_i = 1024, 1280, 1600, 2000, 2500, 3124, 3900, 4880, 6100, 7624, 9530, 11912, 14890, 18612$ such that $N_{i+1}/N_i =$ (or $\approx$)1.25. In accordance with the natural hypotheses on the behavior of relative errors

$$r_h(v) \sim c_v h^{\lambda(v)}, \quad \max_{v=\rho,u,\varepsilon} r_h(v) \sim ch^{\lambda} \quad \text{as} \quad h \to 0,$$

the practical orders of convergence approximating $\lambda(v)$ and $\lambda$ are calculated as

$$\lambda_{i+1}(v) = \ln \frac{r_{h_i}(v)}{r_{h_{i+1}}(v)} \Big/ \ln \frac{N_{i+1}}{N_i}, \quad \lambda_{i+1} = \ln \frac{\max_{v=\rho,u,\varepsilon} r_{h_i}(v)}{\max_{v=\rho,u,\varepsilon} r_{h_{i+1}}(v)} \Big/ \ln \frac{N_{i+1}}{N_i},$$

with $0 \le i \le 12$. The results of computations are given in Figure 2.

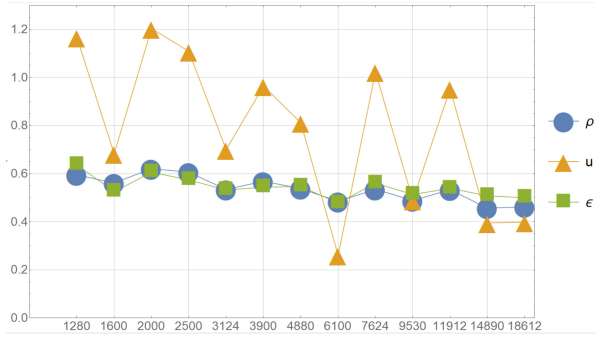


**Figure 2.** Test 1. The practical orders of convergence $\lambda_{i+1}(v)$, $v = \rho, u, \varepsilon$, in dependence on $N_{i+1}$, $0 \le i \le 12$

It should be noticed that $\lambda_i(\rho)$ and $\lambda_i(\varepsilon)$ fluctuate moderately within respectively $[0.456, 0.621]$ and $[0.478, 0.637]$ and differ little from each other, whereas $\lambda_i(u)$ varies quite strongly within $[0.260, 1.204]$ despite the moderate growth of $N_i$.

We emphasize that in this test it turned out that $\max_{v=\rho,u,\varepsilon} r_{h_i}(v) = r_{h_i}(\varepsilon)$ for all $i$. Therefore $\lambda_i = \lambda_i(\varepsilon)$ for all $i$, and this value tends to $\approx 0.5$ as $i$ grows.

*Test 2.* In this flow, two rarefaction waves are formed running away from the region center $x = 0$, where $\rho$ and $p$ are close to 0 (in particular, $\rho(0, t_{fin}) \approx 0.022$ and $p(0, t_{fin}) \approx 0.0019$) but $\varepsilon$ does not tend to zero. Although the solution is continuous for $t > 0$, for a lot of schemes [12], including the scheme $S_0$ [4,5] and the QGD-scheme in [9], a significant unphysical local extremum of $\varepsilon$ (an entropy wake) is observed for $x = 0$, which slowly decreases as $N$ grows.

The results of computations are presented in Figure 3. The entropy wake is almost insignificant there. Moreover, it slowly decreases and contracts as $N$ grows. The solution is still computed for $\beta = 0.6$, but its quality decreases as $\beta$ grows, and at $\beta = 0.7$ it is already destroyed.

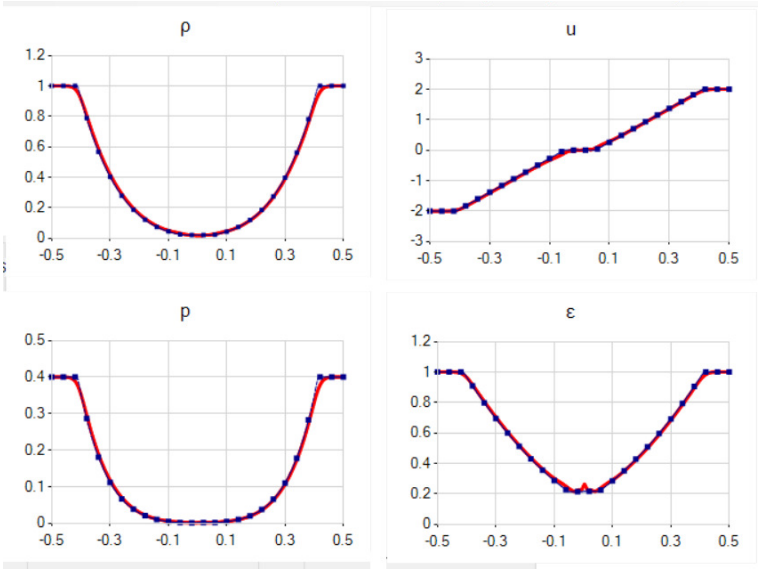


**Figure 3.** Test 2. Solutions for $\alpha = 0.018$, $\beta = 0.2$ and $N = 250$

For the schemes $\mathcal{A}$ and $\mathcal{B}$, the results are similar. For the scheme $\mathcal{A}_1$, the quality of computing $u$ and $\varepsilon$ in the vicinity of $x = 0$ is worse; for the scheme $\mathcal{A}_2$, it is quite low (with large wakes not only in $\varepsilon$ but $\rho$ as well). For the scheme $\mathcal{S}$, even for a small $\beta = 0.01$, the solution is destroyed; if, for example, $\alpha = \beta = 0.1$, then the solution is computed, but its quality is low.

We can improve further the numerical solution applying the refined mesh on $[-0.1, 0.1]$. In particular, diminishing the step 4 times there and thereby increasing $N$ up to 400, we reduce both the height and especially the support of the entropy wake in $\varepsilon$.

*Test 3.* The gas flow consists of two shock waves diverging in gas between which a contact discontinuity moves. The maxima of $\rho$ and $p$ increase substantially. The results of computations are presented in Figure 4.

For the schemes $\mathcal{A}$ and $\mathcal{B}$, the results are similar. For the schemes $\mathcal{A}_1$, $\mathcal{A}_2$ and $\mathcal{S}$, hollows of $\rho$ and $p$ are observed before the front of the left shock wave. For the scheme $S_0$, $\alpha = 0.4$ and lesser $\beta = 0.1$ were taken, and the quality of the numerical solution was somewhat worse [5].

*Test 4.* The flow contains a strong shock wave, a rarefaction wave and a contact discontinuity between them. A narrow and high local maximum (a peak) of $\rho$ arises, and its accurate reproduction requires to use large $N$. There are also known difficulties [4, 5, 12] in computing $u$ in the vicinity of the rarefaction wave $x \approx -0.32$, where the difference of values of $\rho$ is very small. The results of the computation are shown in Figure 5.

For the schemes $\mathcal{A}$ and $\mathcal{B}$, the results are mainly similar. In particular, for $\alpha = 0.2$ and $N = 6400$, for the scheme $\mathcal{A}$ and the schemes $\mathcal{A}_1$, $\mathcal{A}_2$, $\mathcal{B}$ the values respectively $\beta = 0.3$ and $\beta = 0.2$ are admissible.

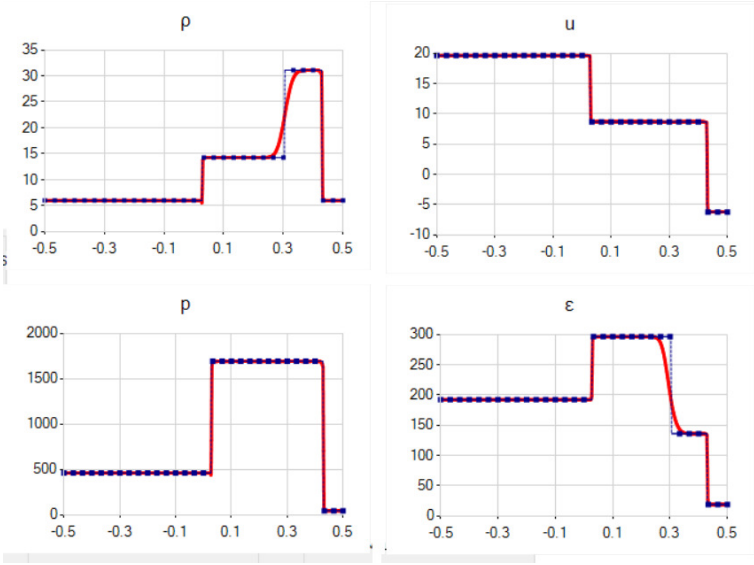


**Figure 4.** Test 3. Solutions for $\alpha = 0.3$, $\beta = 0.5$ and $N = 600$

For the scheme $\mathcal{S}$ and $\alpha = 0.6$ as well as the scheme $S_0$ and $\alpha = 0.3$ [5], the value $\beta = 0.3$ is admissible.

For a non-uniform spatial mesh, the total amount of nodes can be reduced with the same quality of the results. Namely, the same step can be kept in $[0, 0.1]$ but outside this segment it can be taken larger so that the total amount of nodes will be $N = 3000$.

*Tests 5a and 5b.* The initial data of these tests are characterized by a high jump in $u$ but constant $|u|$ and $\varepsilon$ and differ only by a 2- or 20-fold jumps in $\rho$. The results of computations in the simpler test 5a are omitted for brevity, and in the more complex test 5b they are presented in Figure 6.

For the schemes $\mathcal{A}$ and $\mathcal{B}$, the results in both tests 5a and 5b are similar. In particular, for $N = 500$, in the tests 5a and 5b, the values respectively $\alpha = 0.4$ and $\beta = 0.1$ as well as $\alpha = \beta = 0.2$ are admissible. As for the schemes $\mathcal{S}$, $\mathcal{A}_1$ and $\mathcal{A}_2$, the solutions *are destroyed* in both tests even for a much smaller $\beta = 0.001$. Also, for the scheme $S_0$ and QGD-scheme from [9], there exist serious problems concerning the computation of solutions (M.V. Kraposhin, private communication).

In addition to the above tests, successful computations of many other tests known in the literature were performed. Their results are omitted for brevity.

Thus, for the schemes $\mathcal{A}$ and $\mathcal{B}$ the results are mostly close, and they well proven themselves in the test computations and in some of them demonstrated obtaining numerical solutions of better quality (on the same grid) and/or the possibility of using a larger (sometimes hundreds of times) time step than for the standard-type QGD-schemes. In some tests, the simplified schemes $\mathcal{A}_1$ and $\mathcal{A}_2$ are significantly inferior to the scheme $\mathcal{A}$ and thus such simplifications are not always justified.

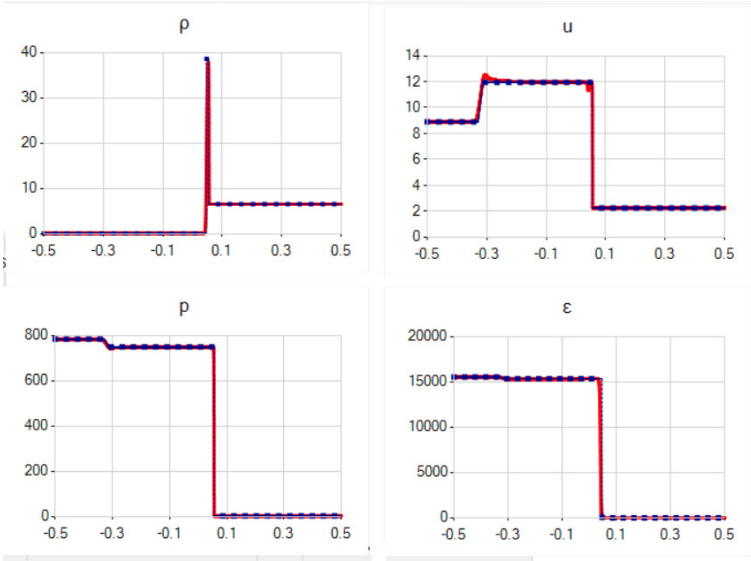


**Figure 5.** Test 4. Solutions for $\alpha = 0.2$, $\beta = 0.2$ and $N = 6400$

## 4 Analysis of relevance in the nonlinear statement of linearized $L^2$-dissipativity conditions

Both necessary and sufficient conditions have recently been derived in [22] for $L^2$-dissipativity of the Cauchy problem for the scheme $\mathcal{S}$ linearized at a constant background solution $(\rho, u, \varepsilon) = (\rho_*, u_*, \varepsilon_*)$, with $\rho_* > 0$ and $\varepsilon_* > 0$.

Using formula (2.8)(b) for $\tau$, the necessary condition for the scheme $\mathcal{S}$ and the schemes $\mathcal{A}$ and $\mathcal{B}$ has the same form

$$\beta \le \widehat{\beta}_{nec}(\widehat{\alpha}, M) := \min\big\{2\widehat{\alpha}, (M+1)^2/\big[2\widehat{\alpha}\big(M^2 + \underline{\lambda}_{\max}\big)\big]\big\}, \qquad (4.1)$$

where $M = |u_*|/c_{s*}$ and $c_{s*} = \sqrt{\gamma(\gamma-1)\varepsilon_*}$ are the background Mach number and sound velocity as well as

$$\underline{\lambda}_{\max} = \max\Big\{\frac{\widehat{\alpha}_P + 1}{2} + \Big[\Big(\frac{\widehat{\alpha}_P - 1}{2}\Big)^2 + \frac{\gamma-1}{\gamma}\widehat{\alpha}_P\Big]^{1/2},$$
$$\frac{(\alpha_S+1)/\gamma + 1}{2} + \Big[\Big(\frac{(\alpha_S-1)/\gamma + 1}{2}\Big)^2 + \frac{4}{\gamma}M^2\Big]^{1/2},$$
$$\frac{(\alpha_S-1)/\gamma + \widehat{\alpha}_P}{2} + 1 + \Big[\Big(\frac{\widehat{\alpha}_P - (\alpha_S+1)/\gamma}{2}\Big)^2 + 4\frac{\gamma-1}{\gamma}M^2\Big]^{1/2}\Big\},$$

with $\widehat{\alpha}_P = 1/\alpha_P$.

If formula (2.8)(a) for $\tau$ is in use, then condition (4.1) takes the form

$$\beta \le \beta_{nec}(\alpha, M) := \min\big\{2\alpha(M+1), (M+1)/\big[2\alpha\big(M^2 + \underline{\lambda}_{\max}\big)\big]\big\}. \qquad (4.2)$$

Comparison of conditions (4.1) and (4.2) gives arguments in favor of formula (2.8)(b) for large $M$ [22].

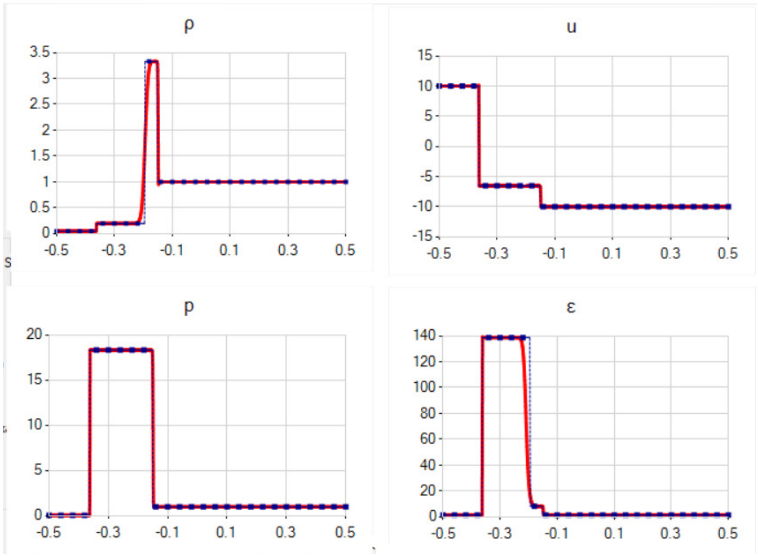


**Figure 6.** Test 5b. Solutions for $\alpha = 0.4$, $\beta = 0.1$ and $N = 500$

The question to what extent the conditions are relevant in the nonlinear statement including the case of the growing Mach number is of great interest. In order to analyze it, numerical experiments were performed for the model Riemann problem with the values $\rho_L = 0.5$, $u_L = \sqrt{\gamma} M_0$, $p_L = 0.5$, $\rho_R = 1$, $u_R = 0$ and $p_R = 1$ as well as $\gamma = 5/3$ (note that $\varepsilon_L = \varepsilon_R = 3/2$), $X = 1$ and $t_{fin} = 0.03$. The values of the "left" Mach number $M_0 = 2, 4, 6$ were taken.

Both formulas (2.8)(b) and (2.8)(a) were used, and the values respectively $\widehat{\alpha} = 0.2, 0.3, \ldots, 0.9$ and $\beta = 0.1k\widehat{\beta}_{nec}(\widehat{\alpha}, M_0)$ as well as $\alpha = 0.1, 0.2, \ldots, 0.9$ and $\beta = 0.1k\beta_{nec}(\alpha, M_0)$, $1 \le k \le 11$, were tested.

To analyze the quality of numerical solutions, we applied (similarly to [23]) the deviation of their relative variation from 1 at the time moment $t = t_{fin}$:

$$\delta_V = \max_{v=\rho,u,\varepsilon} \left| \frac{V_h(v)}{V(v_{ex})} - 1 \right| \quad \text{with} \quad V_h(v) := \sum_{k=1}^{N} |v_k - v_{k-1}|.$$

Here $V_h(v)$ is the variation on the mesh $\omega_{Xh}$ of the approximate function $v$, and $V(v_{ex})$ is the variation on $[-X/2, X/2]$ of the related exact function $v_{ex}$.

The results of computations are presented for the scheme $\mathcal{B}$ in Figures 7 and 9, respectively, for formulas (2.8)(b) and (2.8)(a), as well as for the scheme $\mathcal{S}$ in Figure 8 for formula (2.8)(b). We take $N = 1000$. The upper and lower $\Lambda$-shaped lines depict plots of the right-hand sides of the necessary conditions (4.1) and (4.2) for $M = M_0$ and $M = 0$ respectively; here they are broader for $M = M_0$ than for $M = 0$.

The points with $\delta_V \in [0, 0.1]$, $(0.1, 0.2]$ and $(0.2, \infty]$ are marked with triangles, squares and circles respectively; here $\delta_V = \infty$ and the dash in the tables below mean that the solution was destroyed due to overflow or the values $\rho < 0$

or $\varepsilon < 0$ were obtained. Conditionally, one may consider the points with such $\delta_V$ corresponding to stable, intermediate and unstable solutions, respectively, since the plots of the first ones can include only single hollows or spikes, quite acceptable in practice, whereas the plots of the third type solutions, on the contrary, contain noticeable oscillations as a rule.

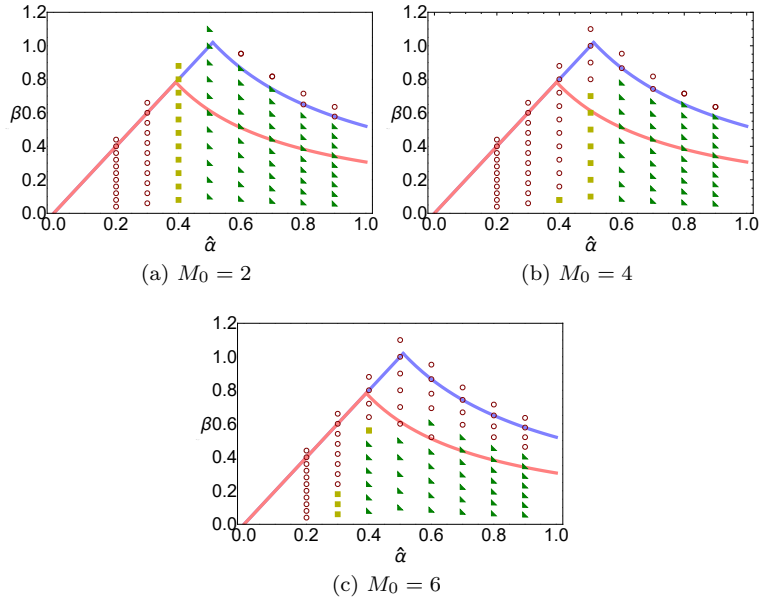


(a) $M_0 = 2$ (b) $M_0 = 4$

(c) $M_0 = 6$

**Figure 7.** Practical stability analysis of the scheme $\mathcal{B}$ for $\beta = 0.1k\widehat{\beta}_{nec}(\widehat{\alpha}, M_0)$, $1 \le k \le 11$, in dependence on $\widehat{\alpha}$, for $M_0 = 2, 4, 6$ and $\tau = \widehat{\alpha}h/(|u| + c_s)$

In Figure 7, for $M_0 = 2$ and $\widehat{\alpha} \ge 0.4$ as well as $M_0 = 4$ and $\widehat{\alpha} \ge 0.5$, the results correspond well to condition (4.1) for $M = M_0$; if $M_0 = 6$ and $\widehat{\alpha} \ge 0.4$, then they correspond better to condition (4.1) for $M = 0$. All computations for $\widehat{\alpha}$ and $\beta$ violating condition (4.1) for $M = M_0$ are unstable excluding the only case $M_0 = 2$ and $\widehat{\alpha} = 0.5$.

In addition, in the Table 2, the values $\delta_V$ are given in dependence on $\widehat{\alpha}$ and $k$, i.e. $\beta$, for $M_0 = 6$. Note that they are non-decreasing in $k$ for all $\widehat{\alpha}$, excluding $\widehat{\alpha} = 0.4$, where they first decrease to $k = 4$, and $\widehat{\alpha} = 0.6$, where for $k = 6$ the solution is destroyed but for the next $k = 7$ the solution is computed again. The latter is rather curious and shows how complicated can be situation with stability in nonlinear statement. For $k = 9, 10, 11$ and all $\widehat{\alpha}$ the solutions are destroyed; the same takes place already for $k = 8$ and $\widehat{\alpha} \ne 0.3$. The values $\delta_V$ are minimal for $\widehat{\alpha} = 0.9$ and, moreover, they decrease in $\widehat{\alpha}$ for $1 \le k \le 7$ (ignoring the dashes for $k = 6, 7$).

Comparison of Figures 7 and 8 shows that, for $M_0 = 6$ as well as $M_0 = 4$ and $\widehat{\alpha} \ge 0.6$, the results for the scheme $\mathcal{B}$ are essentially better than those for the scheme $\mathcal{S}$. For $M_0 = 4$ and $\widehat{\alpha} \le 0.5$, the situation is opposite despite that condition (4.1) is the same for the both schemes.

**Table 2.** The values $\delta_V$ (the scheme $\mathcal{B}$) for various $\widehat{\alpha}$ and $\beta = 0.1k\widehat{\beta}_{nec}(\widehat{\alpha}, M_0)$ and $M_0 = 6$

| $\alpha/k$ | 1 | 2 | 3 | 4 | 5 | 6 | 7 | 8 | 9 | 10 | 11 |
|---|---|---|---|---|---|---|---|---|---|---|---|
| 0.2 | 0.46 | 0.47 | 0.49 | 0.51 | 0.54 | - | - | - | - | - | - |
| 0.3 | 0.16 | 0.18 | 0.19 | 0.22 | 0.24 | 0.26 | 0.29 | 0.31 | - | - | - |
| 0.4 | 0.098 | 0.096 | 0.093 | 0.088 | 0.089 | 0.10 | 0.12 | - | - | - | - |
| 0.5 | 0.067 | 0.069 | 0.070 | 0.071 | 0.071 | - | - | - | - | - | - |
| 0.6 | 0.050 | 0.051 | 0.053 | 0.054 | 0.057 | - | 0.060 | - | - | - | - |
| 0.7 | 0.032 | 0.034 | 0.035 | 0.037 | 0.038 | 0.039 | 0.041 | - | - | - | - |
| 0.8 | 0.016 | 0.017 | 0.018 | 0.020 | 0.021 | 0.022 | 0.023 | - | - | - | - |
| 0.9 | 0.0063 | 0.0064 | 0.0065 | 0.0066 | 0.0067 | 0.0068 | 0.0069 | - | - | - | - |

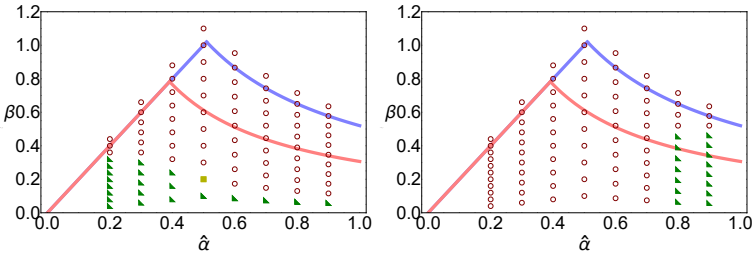


(a) $M_0 = 4$ (b) $M_0 = 6$

**Figure 8.** Practical stability analysis of the scheme $\mathcal{S}$ for $\beta = 0.1k\widehat{\beta}_{nec}(\widehat{\alpha}, M_0)$, $1 \le k \le 11$, in dependence on $\widehat{\alpha}$, for $M_0 = 4, 6$ and $\tau = \widehat{\alpha}h/(|u| + c_s)$

In Figure 9 for $M_0 = 2$ and $\alpha \ge 0.3$ as well as $M_0 = 4, 6$ and $\alpha \ge 0.2$, the results correspond well to condition (4.2) for $M = M_0$. But for $\alpha = 0.1$ (that is the closest value to the maximum point of the right-hand side of (4.2) for $M = 0$ and $M = M_0 = 4, 6$) all the computations are unstable. All numerical results for $\alpha$ and $\beta$ violating condition (4.2) for $M = M_0$ are also unstable.

In addition, in the Table 3, the values $\delta_V$ are given in dependence on $\alpha$ and $\beta$ for $M_0 = 6$. Note that for $\alpha \ne 0.3$ they are non-increasing (though negligibly) as $k$ increases from 1 to 9 that in general is anomalous behaviour. For $\alpha = 0.9$ and $k = 1, 2$, $\delta_V$ even passes the "critical" value 0.1. But, for $\alpha = 0.3$, the values $\delta_V$ are non-decreasing. For $\alpha \ge 0.3$, the values increase with the jump when $k = 9$ changes to 10, and for all $\alpha$ and $k = 11$ the solutions are already destroyed. The values $\delta_V$ are minimal for $\alpha = 0.4$ and, moreover, they decrease in $\alpha = 0.2, 0.3, 0.4$ and increase in $\alpha \ge 0.4$, for all $1 \le k \le 9$.

Thus conditions (4.1) and (4.2) can be also applied in the nonlinear statement as the Mach number grows, within certain limits and at least in some computations. However, as a rule, this is more adequate for the entropy dissipative QGD-discretizations but overestimates the acceptable time step for the standard-type QGD-schemes. Similar conclusions follow from [23] in the simpler barotropic case.

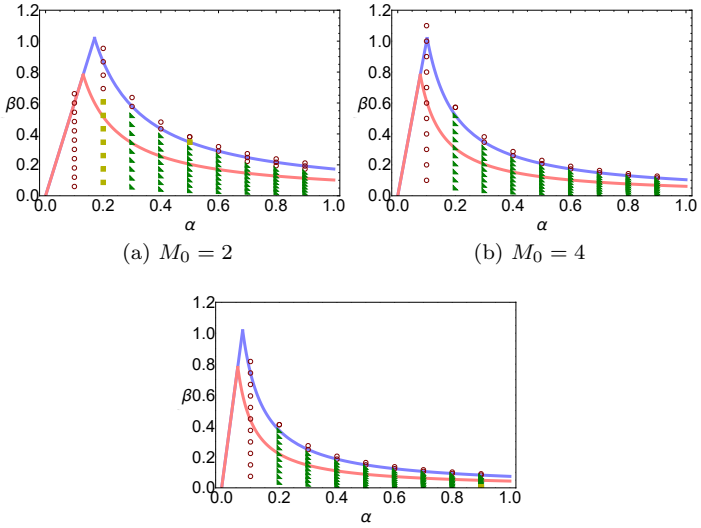


(a) $M_0 = 2$ (b) $M_0 = 4$

(c) $M_0 = 6$

**Figure 9.** Practical stability analysis of the scheme $\mathcal{B}$ for $\beta = 0.1k\beta_{nec}(\alpha, M_0)$, $1 \le k \le 11$, in dependence on $\alpha$, for $M_0 = 2, 4, 6$ and $\tau = \alpha h/c_s$

**Table 3.** The values $\delta_V$ (the scheme $\mathcal{B}$) for various $\alpha$ and $\beta = 0.1k\beta_{nec}(\alpha, M_0)$ and $M_0 = 6$

| $\alpha/k$ | 1 | 2 | 3 | 4 | 5 | 6 | 7 | 8 | 9 | 10 | 11 |
|---|---|---|---|---|---|---|---|---|---|---|---|
| 0.2 | 0.051 | 0.051 | 0.051 | 0.051 | 0.05 | 0.05 | 0.05 | 0.049 | 0.048 | 0.047 | - |
| 0.3 | 0.019 | 0.02 | 0.02 | 0.021 | 0.021 | 0.022 | 0.022 | 0.023 | 0.023 | 9.2 | - |
| 0.4 | 0.0084 | 0.0081 | 0.0079 | 0.0076 | 0.0073 | 0.0070 | 0.0068 | 0.0065 | 0.0062 | 17 | - |
| 0.5 | 0.024 | 0.023 | 0.023 | 0.023 | 0.023 | 0.023 | 0.022 | 0.022 | 0.022 | 9.3 | - |
| 0.6 | 0.039 | 0.039 | 0.039 | 0.039 | 0.039 | 0.038 | 0.038 | 0.038 | 0.038 | 5.1 | - |
| 0.7 | 0.056 | 0.056 | 0.055 | 0.055 | 0.055 | 0.055 | 0.055 | 0.055 | 0.054 | 27 | - |
| 0.8 | 0.089 | 0.072 | 0.072 | 0.072 | 0.072 | 0.072 | 0.071 | 0.071 | 0.071 | 18 | - |
| 0.9 | 0.12 | 0.089 | 0.088 | 0.088 | 0.088 | 0.088 | 0.088 | 0.088 | 0.088 | 30 | - |

## Acknowledgements

The study was presented at the 23$^{\text{th}}$ International Conference on Mathematical Modelling and Analysis, Sigulda, 2018. It was partially supported by the RFBR, project nos. 18-01-00587 and 19-01-00262 as well as within the framework of the Basic Research Program at the National Research University Higher School of Economics (HSE) and a subsidy by the Russian Academic Excellence Project '5-100'.

## References

[1] R. Abgrall and C.-W. Shu(Eds.). *Handbook of numerical methods for hyperbolic problems: basic and fundamental issues.* North Holland, Amsterdam, 2016.

https://doi.org/10.1016/s1570-8659(16)x0002-6.

[2] B.N. Chetverushkin. *Kinetic schemes and quasi-gas dynamic system of equations.* CIMNE, Barcelona, 2008.

[3] T.G. Elizarova. *Quasi-gas dynamic equations.* Springer, Dordrecht, 2009. https://doi.org/10.1007/978-3-642-00292-2.

[4] T.G. Elizarova and E.V. Shil'nikov. Capabilities of a quasi-gasdynamic algorithm as applied to inviscid gas flow simulation. *Comput. Math. Math. Phys.*, **49**(3):532–548, 2009. https://doi.org/10.1134/s0965542509030142.

[5] T.G. Elizarova and I.A. Shirokov. *Regularized equations and examples of their using in modeling gas-dynamic flows.* MAKS Press, Moscow, 2017. (in Russian)

[6] U.S. Fjordholm, S. Mishra and E. Tadmor. Arbitrarily high-order accurate entropy stable essentially nonoscillatory schemes for systems of conservation laws. *SIAM J. Numer. Anal.*, **50**:544–573, 2012. https://doi.org/10.1137/110836961.

[7] V.A. Gavrilin and A.A Zlotnik. On spatial discretization of the one-dimensional quasi-gasdynamic system of equations with general equations of state and entropy balance. *Comput. Math. Math. Phys.*, **55**(2):264–281, 2015. https://doi.org/10.1134/s0965542515020098.

[8] S.K. Godunov and I.M. Kulikov. Computation of discontinuous solutions of fluid dynamics equations with entropy nondecrease guarantee. *Comput. Math. Math. Phys.*, **54**(6):1012–1024, 2014. https://doi.org/10.1134/s0965542514060086.

[9] M.V. Kraposhin, E.V. Smirnova, T.G. Elizarova and M.A. Istomina. Development of a new OpenFOAM solver using regularized gas dynamic equations. *Comput. Fluids*, **166**:163–175, 2018. https://doi.org/10.1016/j.compfluid.2018.02.010.

[10] A.G. Kulikovskii, N.V. Pogorelov and A.Yu. Semenov. *Mathematical aspects of numerical solution of hyperbolic systems.* Chapman&Hall/CRC, London, 2001.

[11] R.J. LeVeque. *Finite volume methods for hyperbolic problems.* Cambridge University Press, Cambridge, 2004. https://doi.org/10.1017/cbo9780511791253.005.

[12] R. Liska and B. Wendroff. Comparison of several difference schemes on 1D and 2D test problems for the Euler equations. *SIAM J. Sci. Comput.*, **25**(3):995–1017, 2003. https://doi.org/10.1007/978-3-642-55711-8_78.

[13] G.P. Prokopov. Necessity of entropy control in gasdynamic computations. *Comput. Math. Math. Phys.*, **47**(9):1528–1537, 2007. https://doi.org/10.1134/s0965542507090138.

[14] M. Svärd and H. Özcan. Entropy stable schemes for the Euler equations with far-field and wall boundary conditions. *J. Sci. Comput.*, **58**(1):61–89, 2014. https://doi.org/10.1007/s10915-013-9727-7.

[15] E. Tadmor. Entropy stability theory for difference approximations of nonlinear conservation laws and related time-dependent problems. *Acta Numer.*, **12**:451–512, 2003. https://doi.org/10.1017/cbo9780511550157.007.

[16] E.F. Toro. *Riemann solvers and numerical methods for fluid dynamics, 3rd ed.* Springer, Berlin, 2009. https://doi.org/10.1007/978-3-662-03915-1.

[17] A.R. Winters and G.J. Gassner. Affordable, entropy conserving and entropy stable flux functions for the ideal MHD equations. *J. Comput. Phys.*, **304**:72–108, 2016. https://doi.org/10.1016/j.jcp.2015.09.055.

[18] A.A. Zlotnik. Quasi-gasdynamic system of equations with general equations of state. *Dokl. Math.*, **81**(2):312–316, 2010. https://doi.org/10.1134/s1064562410020419.

[19] A.A. Zlotnik. Spatial discretization of the one-dimensional quasi-gasdynamic system of equations and the entropy balance equation. *Comput. Math. Math. Phys.*, **52**(7):1060–1071, 2012. https://doi.org/10.1134/s0965542512070111.

[20] A.A. Zlotnik. Entropy-conservative spatial discretization of the multidimensional quasi-gasdynamic system of equations. *Comput. Math. Math. Phys.*, **57**(4):706–725, 2017. https://doi.org/10.1134/s0965542517020166.

[21] A.A. Zlotnik and B.N. Chetverushkin. Parabolicity of the quasi-gasdynamic system of equations, its hyperbolic second-order modification, and the stability of small perturbations for them. *Comput. Math. Math. Phys.*, **48**(3):420–446, 2008. https://doi.org/10.1134/s0965542508030081.

[22] A.A. Zlotnik and T.A. Lomonosov. On conditions for $L^2$-dissipativity of linearized explicit QGD–finite-difference schemes for the equations of one-dimensional gas dynamics. *Dokl. Math.*, **98**(2):458–463, 2018. https://doi.org/10.1134/S1064562418060200.

[23] A.A. Zlotnik and T.A. Lomonosov. Conditions for $L^2$-dissipativity of linearized explicit finite-difference schemes with regularization for the equations of 1D barotropic gas dynamics. *Comput. Math. Math. Phys.*, **59**, 2019. (accepted)